

Expansion and Hadronization of a Chirally Symmetric Quark–Meson Plasma

P. Rehberg, L. Bot and J. Aichelin

SUBATECH

Laboratoire de Physique Subatomique et des Technologies Associées

UMR Université de Nantes, IN2P3/CNRS, Ecole des Mines de Nantes

4 Rue Alfred Kastler, F-44070 Nantes Cedex 03, France

Abstract

Using a chirally symmetric Lagrangian, which contains quarks as elementary degrees of freedom and mesons as bound states, we investigate the expansion and hadronization of a fireball, which initially contains only quarks and produces mesons by collisions. For this model, we study the time scales of expansion and thermal and chemical equilibration. We find that the expansion progresses relatively fast, leaving not necessarily enough time to establish thermal and chemical equilibrium. Mesons are produced in the bulk of the fireball rather than at a surface, at a temperature below the Mott temperature. Initial density fluctuations become amplified during the expansion. These observations challenge the applicability of hydrodynamical approaches to the expansion of a quark-gluon plasma.

PACS numbers: 25.75.-q, 12.28.Mh, 12.39.Fe, 24.10.Lx

Typeset using REVTeX

I. INTRODUCTION

The physics of the quark-gluon plasma (QGP) has formed one of the most important points of interest in nuclear and high energy physics during the last years [1]. While possible evidence for its creation has already been obtained in $Pb-Pb$ collisions at the CERN SPS, new experiments at RHIC and LHC are under construction. It is expected that these experiments will reproduce the SPS results and beyond that confirm other signals for the creation of a QGP, which have been proposed in the literature.

With these improved experiments coming up soon, there is a clear need for a theoretical description, which is able to describe the different stages of a heavy ion collision, as there are (i) the formation of the fireball, (ii) its expansion within the QGP phase, (iii) the phase transition to the hadronic phase, (iv) the expansion within the hadronic phase, and (v) the decay of the fireball into noninteracting fragments. With the exception of the first of these stages, this is frequently done using hydrodynamical models [2] due to the lack of a more realistic approach. This approach assumes, that one has local thermal equilibrium during the whole evolution at least for the light and thus dominant components of the system, so that it is sufficient to compute the space-time dependence of the energy-momentum tensor using a phenomenological equation of state, which may be extracted e.g. from lattice simulations. One of the drawbacks of this method is that it is implicitly assumed that the time scale for collisions is short compared to the expansion time scale, which is by no means obvious due to the large expansion velocity of the fireball. Furthermore, the equation of state is unknown for $\mu = 0$, since this sector is still not accessible for lattice computations. Another weak point is that hydrodynamics has no intrinsic freezeout mechanism, so that the breakup stage into hadrons of the expansion must be described by additional assumptions.

Another common approach for the modelization of heavy ion collisions are transport calculations based on cascade codes. These models have the advantage of being generic non-equilibrium calculations. They suffer, however, from the fact that usually the in-medium modifications of particle properties and interaction cross sections are neglected. Furthermore, no attempt is made to apply these calculations to phase transitions. This limits the validity of these models to the late stages of the expan-

sion, where the system is already in the hadronic phase.

The approach we present here differs from those presented above in that we attempt to construct a cascade type model, which is nevertheless able to describe a transition from a pure quark phase to a hadronic phase, and which also takes into account the in-medium modifications of quark and hadron properties. Doing this in a fashion which describes all of the phenomena is nevertheless impossible, since one of the major effects of the QGP transition, the confinement, is presently not understood sufficiently to implement it in a non-equilibrium model. It is, however, known that confinement does not play an important role in the low energy hadron phenomenology. This sector is rather dominated by chiral symmetry, which can be well described by effective models. Since the importance of chiral symmetry is well established and the behaviour of effective chiral models is also extensively studied, an incorporation of this symmetry into the dynamical theory of heavy ion collisions seems mandatory. We thus take one of these effective models, the Nambu–Jona-Lasinio (NJL) model [3,4], for which a non-equilibrium treatment has been recently derived [5–9], and for which first numerical solutions have been reported in Refs. [8,10,11]. The advantages of this approach are obvious: Since the NJL model starts from a Lagrangian, which contains only quarks as elementary degrees of freedom and treats pions as bound states, one is able to describe the transition of a hot system containing only quarks initially to a system which contains quarks and hadrons. The technical tools for the treatment of this transition have been developed in Ref. [9]. The possibility of including both quarks and hadrons, the former appearing in the initial state while the latter will be present in the final state, distinguishes the NJL model from most of the other chiral models such as chiral perturbation theory or the σ -model [12], while the description of hadronic properties at low temperatures is equally good for all of them. A comparison of the NJL mesonic mass spectrum with the lattice calculations of Ref. [13] shows that also at high temperatures the NJL model provides a good description of mesonic properties. Besides that, another advantage of our approach is that it is possible to derive the whole expansion scenario from one single Lagrange density. Since the NJL model does, however, not include confinement, a price has to be paid for this, in that the transition between the two phases is not given by a confinement transition, but rather by a Mott effect [14]. As a consequence, one has thus free quarks at all

temperatures.

The numerical method we choose for the solution of the transport equations is an algorithm of the QMD type [15]. In this approach, it is assumed that the particles can be described by (nonrelativistic) gaussian wave functions, which contain two time dependent parameters, the position of the centroids in coordinate and momentum space. The total wavefunction of the system is assumed to be the product of the wave function of the individual particles. The form of the wavefunction remains time independent and the time evolution of the parameters is obtained applying a time dependent variational principle, which yields time evolution equations very close to the classical time evolution equations. Being a n -body theory, this approach allows to investigate in detail the time evolutions of correlations and fluctuations, which is beyond the range of applicability of BUU type transport theories. For details we refer the reader to Ref. [16].

Previous approaches to a nonequilibrium treatment of the NJL model have been given in Refs. [8,10,11]. This work goes beyond Refs. [10,11] in that these papers only considered a system of quarks moving within a mean field, whereas we consider also collisions. Reference [8] also included collisions in a relaxation time approach, however, mesonic degrees of freedom and the mechanisms of their creation were not studied there. This is thus the first work, in which the chiral phase transition is studied including collisions between quarks as well as a hadronization of quarks into mesons.

This paper is organized as follows: In Sec. II, we describe our interaction model and its numerical treatment. Numerical results are given in Sec. III. We summarize and conclude in Sec. IV.

II. DESCRIPTION OF THE MODEL AND THE ALGORITHM

The model which we use throughout this paper is the Nambu–Jona-Lasinio (NJL) model [3] in its two flavor version, which is defined by the Lagrangian

$$\mathcal{L} = \bar{\psi} (i \not{\partial} - m_0) \psi + G \left[\left(\bar{\psi} \psi \right)^2 + \left(\bar{\psi} i \gamma_5 \vec{\tau} \psi \right)^2 \right] . \quad (2.1)$$

Here, ψ denotes the quark fields, which are implicitly understood to carry flavor and color indices, and $\vec{\tau}$ are the Pauli matrices in flavor space. A current quark mass m_0 is introduced, which provides a small explicit chiral symmetry breaking.

For a review of the equilibrium properties of this model, the reader is referred to Ref. [4]. Here we summarize only those points, which are essential for our calculations. At small temperatures and densities, the interaction in Eq. (2.1) leads to a spontaneous breakdown of chiral symmetry, which is described by a finite effective quark mass m_q . To lowest order in an expansion in the inverse number of colors, $1/N_c$ [17], which for quarks is commensurate with the Hartree approximation, m_q is given by the gap equation

$$m_q = m_0 + 2Gm_q \int_{|\vec{p}| < \Lambda} \frac{d^3p}{(2\pi)^3} \frac{1}{E_q(\vec{p})} (2N_c N_f - n_q(\vec{p}) - n_{\bar{q}}(\vec{p})) \quad , \quad (2.2)$$

where $E_q(\vec{p}) = \sqrt{\vec{p}^2 + m_q^2}$ is the quasiparticle energy of the quarks and $n_q(\vec{p})$, $n_{\bar{q}}(\vec{p})$ denote the quark and antiquark momentum distributions, respectively. Since the NJL model is non-renormalizable, we have restricted the integral in Eq. (2.2) to momenta smaller than a cutoff Λ .

Pions appear in the NJL model as bound states of quarks and antiquarks in the pseudoscalar interaction channel. As a consequence of the Goldstone theorem, they become massless in the chiral limit, $m_0 \rightarrow 0$. If, however, m_0 is finite, they also acquire a finite mass. Their quasiparticle energy can be extracted from the poles of their effective retarded propagator, $\Delta_\pi^R(p_0, \vec{p})$, which is given by [4]

$$\Delta_\pi^R(p_0, \vec{p}) = \frac{2G}{1 - 2G\Pi_{PS}^R(p_0, \vec{p})} \quad , \quad (2.3)$$

where $\Pi_{PS}^R(p_0, \vec{p})$ is the irreducible retarded pseudoscalar polarization function. The quasiparticle energy of the pion is thus given as the solution of

$$1 - 2G\Pi_{PS}^R(E_\pi(\vec{p}), \vec{p}) = 0 \quad . \quad (2.4)$$

In the following we will make the approximation $E_\pi(\vec{p}) = \sqrt{\vec{p}^2 + m_\pi^2}$, where m_π is computed as $E_\pi(\vec{0})$ from Eq. (2.4). The retarded polarization is computed, again to lowest order in $1/N_c$, from the diagram given in Fig. 1. In this case, the irreducible pseudoscalar polarization is explicitly given by

$$\Pi_{PS}^R(p_0, \vec{p}) = \frac{2 \int_{|\vec{q}| < \Lambda} \frac{d^3q}{(2\pi)^3} \frac{2N_c N_f - n_q(\vec{q}) - n_{\bar{q}}(\vec{q})}{E_q(\vec{q})} \frac{\vec{p}\vec{q}(p^2 + 2\vec{p}\vec{q}) - 2p_0^2 E_q(\vec{q})^2}{(p^2 + 2\vec{p}\vec{q})^2 - 4p_0^2 E_q(\vec{q})^2 + i\epsilon p_0}} \quad , \quad (2.5)$$

with the term $i\epsilon p_0$ in the denominator taking care of the causal structure.

Due to the scalar coupling channel in the Lagrangian (2.1), the model contains also a scalar resonance, the σ meson. Its mass can be computed from a dispersion relation similar to Eq. (2.4), replacing the pseudoscalar polarization by the scalar one,

$$\Pi_S^R(p_0, \vec{p}) = 2 \int_{|\vec{p}| < \Lambda} \frac{d^3 q}{(2\pi)^3} \frac{2N_c N_f - n_q(\vec{q}) - n_{\bar{q}}(\vec{q})}{E_q(\vec{q})} \frac{(\vec{p}\vec{q} + 2m_q^2)(p^2 + 2\vec{p}\vec{q}) - 2p_0^2 E_q(\vec{q})^2}{(p^2 + 2\vec{p}\vec{q})^2 - 4p_0^2 E_q(\vec{q})^2 + i\epsilon p_0} \quad (2.6)$$

This function is computed from the same graph as given in Fig. 1, with $i\gamma^5\tau$ replaced by one.

The mass spectrum computed from Eqs. (2.2), (2.4) in thermal equilibrium is shown in Fig. 2. The parameters used for this plot are $m_0 = 4 \text{ MeV}$, $G\Lambda^2 = 1.989$ and $\Lambda = 820 \text{ MeV}$. At zero temperature, chiral symmetry is spontaneously broken and the quarks appear as constituent quarks with masses of $m_q = 323 \text{ MeV}$. As a consequence, light Goldstone pions appear as bound states, which are, in the chiral limit, massless, but for the parameters given have the mass $m_\pi = 136 \text{ MeV}$. The σ meson has a mass of $m_\sigma = 653 \text{ MeV}$. As the temperature rises, the Pauli blocking term of Eq. (2.2) becomes more and more important. Thus the quark mass drops at high temperatures and chiral symmetry becomes restored. Concomitantly, the pion mass will rise, so that at the Mott temperature T_M its mass becomes equal to that of its constituents, $m_\pi(T_M) = 2m_q(T_M)$. For our parameter set, this transition occurs at $T_M = 219 \text{ MeV}$. At temperatures higher than T_M , the ground state of the model is no longer given by the pions, but rather by the quarks, while the pions themselves become unstable resonances. This instability models, to a certain extent, the deconfinement transition of QCD. For a more detailed discussion of this Mott transition the reader is referred to Ref. [14]. As a consequence of chiral symmetry restauration, the σ mass becomes degenerate with the pion mass at high temperatures.

It has been detailed in Refs. [5–7,9], how the treatment of the NJL model is generalized to non-equilibrium. In particular, it has been shown, that the quasiparticle energy of the quarks is given by an equation similar to Eq. (2.2), where m_q and the momentum distributions become space-time dependent, whereas the meson self energy in turn is given by to Eq. (2.4) with a space-time dependent polarization. The equations of motion for the one particle distribution functions is then given by

$$\left(\partial_t + \vec{\partial}_p E_q \vec{\partial}_x - \vec{\partial}_x E_q \vec{\partial}_p\right) n_q(t, \vec{x}, \vec{p}) = I_{\text{coll},q}[n_q, n_\pi] \quad (2.7a)$$

$$\left(\partial_t + \vec{\partial}_p E_\pi \vec{\partial}_x - \vec{\partial}_x E_\pi \vec{\partial}_p\right) n_\pi(t, \vec{x}, \vec{p}) = I_{\text{coll},\pi}[n_q, n_\pi] \quad , \quad (2.7b)$$

where $I_{\text{coll},q}[n_q, n_\pi]$ and $I_{\text{coll},\pi}[n_q, n_\pi]$ are collision integrals of the Boltzmann type.

In the present paper, we solve Eqs. (2.7) using an QMD-like approach. To this end, we replace the one particle distribution function n_q by the parametrization

$$n_q(t, \vec{x}, \vec{p}) = \sum_{i=1}^{N_q} \exp\left(-\frac{[\vec{x} - \vec{x}_i(t)]^2}{2w^2}\right) \exp\left(-\frac{w^2}{2} [\vec{p} - \vec{p}_i(t)]^2\right) \quad (2.8)$$

and analogously the antiquark distribution function $n_{\bar{q}}$ and the pion distribution function n_π . The normalization in Eq. (2.8) is chosen in such a way that

$$\int \frac{d^3x d^3p}{(2\pi)^3} n_q(t, \vec{x}, \vec{p}) = N_q \quad , \quad (2.9)$$

where N_q is the total number of quarks. The center points $\vec{x}_i(t)$, $\vec{p}_i(t)$ in Eq. (2.8) are moving on the characteristics of Eq. (2.7):

$$\frac{d}{dt} \vec{x}_i(t) = \vec{\partial}_p E \quad (2.10a)$$

$$\frac{d}{dt} \vec{p}_i(t) = -\vec{\partial}_x E + \text{collision contributions} \quad . \quad (2.10b)$$

The second term on the right hand side of Eq. (2.10b) serves to describe the effects of the collision integral. It is computed as follows: for each pair of particles, the coordinates and momenta are boosted into the respective two particle center of mass frame. Here, the distance vector of the particles is decomposed into its longitudinal part, i.e. the part parallel to the relative momentum, and its transverse part, i.e. the part perpendicular to the relative momentum. We decide, which scattering processes are possible for the pair in question and compute the respective cross sections σ_k as well as the total cross section $\sigma_{\text{tot}} = \sum \sigma_k$. A collision happens, if (i) the longitudinal distance of the incoming particles in the CM frame is smaller than the distance traveled by the particle within the time step and (ii) the transverse distance is smaller than $\sqrt{\sigma_{\text{tot}}/\pi}$. In this case, the specific process is chosen with probability $\sigma_k/\sigma_{\text{tot}}$. Neglecting the dependence of the differential cross section on the angles, we choose the direction of the outgoing momenta randomly in the center of mass system and boost them back into the original reference frame.

The processes implemented so far which are treated in this way belong to two classes. The first of these are elastic scattering processes of the form $qq \leftrightarrow qq$, $q\bar{q} \leftrightarrow q\bar{q}$ and $\bar{q}\bar{q} \leftrightarrow \bar{q}\bar{q}$ [18]. The generic Feynman diagrams of these processes in leading order of the $1/N_c$ expansion are shown in Fig. 3. One has two interaction channels, which both proceed via the exchange of a scalar or pseudoscalar meson. The typical cross section for these processes are of the order of millibarns. The second class is represented by hadronization processes, $q\bar{q} \leftrightarrow \pi\pi$ [19,20], for which the Feynman diagrams are shown in Fig. 4. Here, one has an s -channel, which proceeds via the exchange of a scalar resonance, and a t - and u -channel. Also here, the typical cross section is of the order of millibarns. For more details and plots of the cross sections, the reader is referred to Refs. [18–20].

A third class of processes, which cannot be treated by the scheme detailed above, is the decay of pions into two quarks, for which the Feynman diagram is shown in Fig. 5. This process is possible if the pion mass fulfills the Mott condition $m_\pi > 2m_q$ [9]. Here we proceed as follows: first we compute the mean lifetime τ of the pion due to the process $\pi \rightarrow q\bar{q}$. Then we decide with probability $1 - \exp(-\Delta t/\tau)$, where Δt is the time step of the calculation, if the particle decays. In this case we again choose the direction of the outgoing particles randomly in the meson rest frame and boost to the original frame.

In general, the quark and meson quasiparticle energies as well as the scattering cross sections appearing in the collision integrals are complicated functionals of the particle distributions, as can be seen from Eqs. (2.2), (2.4) and the expressions for the cross sections in Refs. [18–20]. An exact computation of these quantities in a non-equilibrium situation is thus a tremendous numerical task. Instead of making an exact computation at each time step, we thus take a shortcut by defining an effective temperature. This is done as follows: First, the gap equation (2.2) with the parametrization (2.8) inserted is solved exactly at each particle position to give the quark mass field $m_q(\vec{x}, t)$. Then the effective temperature is computed from the condition that the quark mass at the respective point is equal to the equilibrium quark mass computed from the effective temperature:

$$m_q(\vec{x}, t) = m_q^{\text{eq}}(T_{\text{eff}}(\vec{x}, t)) \quad . \quad (2.11)$$

From this effective temperature we compute afterwards the pion mass and the scattering cross sections, using the equilibrium expressions. Note that T_{eff} is not the

thermodynamic temperature, but rather an auxiliary quantity for the computation of meson masses and cross sections. It becomes, however, equal to the thermodynamic temperature if thermal equilibrium is reached.

A similar procedure is used for the mass gradients, which appear in Eq. (2.7). First, we compute $\vec{\partial} m_q$ from an exact differentiation of Eqs. (2.2), (2.8). The pion mass gradient is then computed from

$$\vec{\partial}_x m_\pi(\vec{x}, t) = \frac{dm_\pi^{\text{eq}}(T_{\text{eff}})}{dT} \left(\frac{dm_q^{\text{eq}}(T_{\text{eff}})}{dT} \right)^{-1} \vec{\partial}_x m_q(\vec{x}, t) \quad . \quad (2.12)$$

Note that the second factor on the right hand side of Eq. (2.12) is negative, so that the effective force acting on pions due to the mean field is opposite to the one acting on quarks. With these prescriptions at hand, Eqs. (2.10) are solved to give the time evolution of $\vec{x}_i(t)$, $\vec{p}_i(t)$ and thus the time evolution of the one particle distributions.

The initial condition is chosen in the following way: In the beginning, no pions are present, whereas the number of quarks and the number of antiquarks are equal. The spatial center points of the Gaussians representing the quarks $\vec{x}_i(0)$ are distributed homogeneously within a sphere of radius r_0 . The momenta $\vec{p}_i(0)$, on the other hand, are distributed according to a Fermi distribution at a given temperature T_0 , which is a free parameter, and chemical potential $\mu = 0$. The total number of quarks in the initial state is given by the momentum integral over the Fermi distribution times the volume. Since the NJL model is a low energy theory, the momentum distribution is cut off at $p = \Lambda$.

III. NUMERICAL RESULTS

In this section we show the numerical results of our simulation program. All computations have been performed using the parameter set $m_0 = 4 \text{ MeV}$, $G\Lambda^2 = 1.989$ and $\Lambda = 820 \text{ MeV}$. The width of the Gaussians in Eq. (2.8) was chosen to be $w = 2 \text{ fm}$.

A. Evolution of the Fireball

To give an overview over the time evolution of the fireball, we first describe one specific example of a system with initial radius $r_0 = 7 \text{ fm}$ and initial temperature

$T_0 = 280 \text{ MeV}$. A snapshot of the expansion is shown in Fig. 6. The upper part of Fig. 6 shows the initial state, which consists of a sphere filled up with quarks, which are denoted by dark balls. At this time, the system contains 4684 quarks and antiquarks and has a kinetic energy density of about 1.8 GeV/fm^3 . The bottom part of Fig. 6 shows the same system $25 \text{ fm}/c$ later. At this time, approximately 60% of the quarks have been converted into pions, which are denoted by the light balls. Since the NJL model is not confining, the remaining 40% light quarks will not hadronize and remain present in the final state.

Figure 7 gives the time behaviour of the constituent quark masses, averaged over all solid angles, as a function of r at times $t = 0, 5, 10, 15, 20$ and $25 \text{ fm}/c$. At $t = 0$, all quarks are sitting within a sphere of radius 7 fm . In the center of this sphere, the particle density is maximal and the quark mass is thus low. Towards the surface, the density drops due to the gaussian shape of the distribution function and concomitantly the constituent quark mass rises. Note that the quark mass is only known at the centre points $\vec{x}_i(t)$ of the quark distribution functions and the plot ends thus at $r = 7 \text{ fm}$. For larger values of r , it would continuously rise towards the vacuum value, thus forming a sort of ‘potential well’, as was previously shown in Ref. [8]. At finite times, the system starts to expand due to the thermal motion of the quarks. This expansion first depletes the surface of the fireball, while the particle density in the centre stays high, as can be seen from the plot at $t = 5 \text{ fm}/c$ of Fig. 7. At this time, some quarks have already gained their vacuum mass, while the mass of those quarks, which are in the centre, is approximately unchanged. At later times, when the depletion reaches the centre, the ‘potential well’ begins to flatten, until finally all quarks have the vacuum mass. At this time, the interaction due to the mean field ceases. This behaviour has been observed previously in Refs. [8,10].

The effective temperature, averaged over all solid angles, is shown in Fig. 8. Since this quantity is coupled to the constituent quark mass via Eq. (2.11), it shows qualitatively the same behaviour as Fig. 7. Initially, one has a high temperature region in the centre of the fireball and zero temperature outside. As the expansion progresses, the temperature drops in the centre. At $t = 7 \text{ fm}/c$, the temperature is lower than the Mott temperature at all space points. At $t = 25 \text{ fm}/c$, one arrives at a temperature of approximately 50 MeV , which is sufficiently close to zero to give no mean field contribution any longer.

The result which can be drawn from this behaviour is that the high energy density in the initial state leads to a large expansion velocity, which in turn results in a short lifetime of the plasma. Although the increase of the quark mass should make the expansion slower, this does not make a large effect. Quantitatively, this can be seen from Fig. 9, where the mean radius is shown for three systems with identical initial conditions, but different expansion mechanisms: one with full interaction, one expanding according to a Vlasov equation (i.e. without collisions) and one with no interaction at all. The curves for the interacting systems lie below the one for the interaction free system, thus showing that the growing quark mass leads to a slowing down of the expansion, which is, however, not very strong. In the case of a fully interacting system, some of the quarks are converted into pions, which are not slowed down, so that in this case the mean radius is somewhat larger than in the Vlasov case. One may ask the question whether this short lifetime is a generic result or only a consequence of the approximation of the NJL approach. In view of the high initial energy density and the fact that the quark masses are rather small, it is hard to see how an expansion well below the speed of light can be achieved.

Figure 10 shows the time behaviour of the angular averaged particle densities, both for quarks and for pions. In the initial state at $t = 0$, only quarks are present. At later times, pions are produced and thus contribute also to the particle density.

The time dependence of the particle multiplicities is shown in Fig. 11. Here it can be seen that the production of mesons starts immediately after the beginning of the evolution. The pion multiplicity rises steeply at $t = 0$, while the quark multiplicity goes down. This steep rise can be understood from the observation, that the system is rather dense initially, thus giving rise to a high collision rate. At later times, the multiplicity curves flatten. There are two possible reasons for this flattening: either the back reaction $\pi\pi \rightarrow q\bar{q}$ might become important due to the large abundance of pions or the particle density becomes too low to cause a further change of the multiplicities via collisions. To answer this question, we show in Fig. 12 the number of collisions per unit time, dN_c/dt , as a function of time. It can be seen from this figure, that the vast majority of collisions happen before $t = 10 \text{ fm}/c$. If the reaction $\pi\pi \rightarrow q\bar{q}$ became important, the number of collisions would stay high, while the multiplicities do not change any longer. Thus the reason for the flattening of the multiplicity curves is the breakup of the fireball rather than the approach to chemical

equilibrium.

B. Meson Production Mechanisms

In the last subsection it has been pointed out, that approximately half of the quarks in the system do not hadronize and remain present in the final state. In order to investigate this behaviour further, we have simulated systems with initial radii of 3, 4, 5, 6 and 7 fm. For each initial radius, two runs have been performed. The final multiplicities for each system, averaged over the two runs, are given in Tab. I. It can be seen from this table, that the final state for all these runs contains about 50% of quarks, but it can also be seen, that there is a systematic trend towards a higher pion abundance for larger systems. Whereas one has 42% pions at $r_0 = 3$ fm, the pion abundance rises to 60% at $r_0 = 7$ fm. This can be interpreted as an approach towards chemical equilibrium, which is nevertheless not reached, since in an equilibrated cold system, only pions should be present. The production of pions from quarks, however, takes a finite time. The lifetime of a small expanding fireball is too short to hadronize all quarks into pions without involving confinement. Nevertheless, the lifetime rises with the initial radius, so that more quarks can hadronize for a large system.

The hydrodynamical picture of the plasma expansion relies on the assumption of local thermal equilibrium, which is the limit of infinitely large cross sections of transport theory. In this case, the transition from quark matter to hadronic matter takes place immediately after the temperature drops below the critical temperature. In an expanding finite system, however, one has to take into account that the finite size of the cross section leads to a finite mean free path and the hadronization takes a finite time. To verify whether in our nonequilibrium, finite particle number calculation a comparably strong relation between meson production and temperature as in hydrodynamics is realized, we have plotted in Fig. 13 the creation probability of pions versus the effective temperature. It can be seen that pions are predominantly created at temperatures well *below* the Mott temperature within a range of approximately 50 MeV. This figure should be compared to Fig. 23 of Ref. [20], where it has been shown that the mean time for the conversion of quarks into mesons is minimal within the same temperature range where Fig. 13 shows a maximum of the pion production. This means that the mean free path is minimal below the Mott

temperature and quarks tend to hadronize here. We thus conclude that the finite creation time of mesons cannot be neglected against the expansion time scales of the plasma, i. e. effects of the finite mean free path become important.

This behaviour is consistent with the density curves of Fig. 10. Generally one observes, that in the early stages, when the system is still hot in the center, the meson density is maximal at a finite value of r . At later times, when the temperature in the centre drops below the Mott temperature, one has the situation, that the meson density follows the quark density.

C. Density Fluctuations

The initial conditions used above are, besides statistical fluctuations in the distribution of the particles, spherically symmetric. We see, however, in Fig. 14, where we plot the summed particle densities for quarks and pions along the coordinate axes, both for the initial and final state, that these small fluctuations become amplified during the expansion and that the system does not at all keep the symmetry. This is understandable because the increase of the parton mass with decreasing density is equivalent to an attractive force between them. Therefore partons tend to cluster and the initial fluctuations are the seeds for this clusterization. This observation challenges, like the finite mean free path effects, the possibility to employ hydrodynamical approaches, which are only applicable if initial fluctuations are damped.

D. Variation of Initial Conditions

1. Cylindrical Initial Conditions

The initial conditions given in Sec. II are not the ones one would expect in a heavy ion collision. To come closer to the experimental situation, we made one run with cylindrical initial conditions. The spatial center points in this run are equally distributed within a cylinder which, in longitudinal direction, extends from $-z_{\max} \leq z \leq z_{\max}$ with $z_{\max} = 2$ fm and in transverse direction has a radius of 6 fm. The distribution of the momenta perpendicular to the cylinder axis was chosen to be gaussian

$$p(p_x, p_y) \sim \exp\left(-\frac{p_x^2 + p_y^2}{2(\delta p)^2}\right) \quad (3.1)$$

with width $\delta p = 250 \text{ MeV}$. The distribution along the cylinder axis, however, was chosen to depend linearly on z in such a fashion, that $p_z = \pm\Lambda$ is reached at the cylinder faces at $z = \pm z_{\text{max}}$:

$$p(p_z) = \delta(p_z - \Lambda z/z_{\text{max}}) \quad . \quad (3.2)$$

The total number of particles was 2000, which gives approximately the same particle density in the initial state as for the other runs. After $30 \text{ fm}/c$, 1126 quarks have been converted into mesons, which corresponds to 56% of the total particle number. In Fig. 15, we show the time dependence of the multiplicity. This figure shows the same trend as Fig. 11. The geometry does thus not have a large impact on the particle multiplicities. Figure 16 shows the distribution of the center points $\vec{p}_i(t)$ in rapidity both for the initial and the final state. At $t = 0$, one sees a distribution with two maxima at $y = \pm 1.1$. At $t = 30 \text{ fm}/c$, the quark rapidity distribution has become flatter and narrower, while the meson distribution is flat at midrapidity, but has a larger width than the quark distribution. This comes from the fact that quarks are slowed down during to the expansion and thus move to lower rapidities. Mesons, on the other hand, have a lower mass than quarks at the time of their creation and thus obtain a higher momentum as the incoming quarks. This leads to a spread of their rapidity distribution.

Figure 17 shows the mean transverse momentum as a function of rapidity. Here one encounters the same behaviour as for the particle density, in that the distribution for the mesons is wider than for the quarks. The geometry of the expansion does thus not influence the p_T spectra, but shifts the quarks to midrapidity. It is not very astonishing that mesons have the same mean transverse momentum in midrapidity, because the process $q\bar{q} \rightarrow \pi\pi$ leads to about the same value of p_T .

2. Mixed Temperature Initial Condition

In view of the short lifetime of the fireball, the question arises whether the lifetime is long enough in order to establish thermal equilibrium. For this reason we have studied a spherically symmetric system, in which half of the particles with $r > r_0/2$

obtained a momentum according to a temperature of 180 MeV (‘cold’ particles), whereas the other particle momenta were initialized with a temperature of 280 MeV (‘hot’ particles). If thermal equilibrium was established, the ‘cold’ particles would obtain the same energy as the ‘hot’ particles in the course of the expansion. The result is shown in Fig. 18, where we plot the energy per particle for both subsystems as a function of time. It can be seen, that the energy of the ‘cold’ particles approaches that of the ‘hot’ particles, but stays below. One has thus no complete thermal equilibration. This reflects the already discussed observation that the expansion velocity is very large, too large to produce a global equilibrium.

E. Variation of Hadronization Cross Sections

Since the NJL model is nonconfining, one is faced with the question, if a sufficiently enlarged hadronization cross section could lead to a system, which complete hadronizes into mesons. We thus took the initial conditions of Sec. III D 1 and made several calculations, in which we increased all cross sections of the hadronization type, i.e. the ones for $q\bar{q} \rightarrow \pi\pi$ as well as those for the back reaction $\pi\pi \rightarrow q\bar{q}$, artificially by a constant factor. The result is given in Table II, where we give the particle abundancies in the final state for these runs. One sees that the increased hadronization cross section leads to an increased pion abundance in the final state, but nevertheless not to a complete hadronization.

IV. SUMMARY AND CONCLUSIONS

In this paper, we have studied the expansion and hadronization of systems, which interact according to a chirally symmetric Lagrangian. These calculations cannot serve to reproduce experimental data, since the underlying interaction is not confining. Since, however, chiral symmetry is an decisive feature of hadron phenomenology, it serves nevertheless to address qualitatively several questions, which we believe to persist to more realistic scenarios. One of these points concerns the question of collision and expansion time scales. We find that the expansion and cooling progresses relatively fast, so that the finite time, which is needed to produce particles, cannot be neglected. We obtain the result, that chemical and even thermal

equilibrium are not necessarily established during the expansion.

Another interesting point is the production mechanism of mesons, which is studied here for the first time. We find that mesons are created mainly within a temperature range of approximately 50 MeV below the Mott temperature. This effect can be traced back to a minimum of the mean free path. This feature might persist to a confining scenario, because it is hard to see how, even in a confining theory, pions could be created instantaneously. We also find that mesons are created in the bulk of the fireball rather than at its surface and that at late times the meson density follows the quark density.

Starting from an initially spherically symmetric configuration, we observe that this configuration does not necessarily stay symmetric, but rather tends to form local density maxima at late times. All these last three statements challenge the applicability of hydrodynamical models.

Using a cylindrically symmetric initial configuration, which might be more realistic to encounter in an experimental situation, we find a flat rapidity distribution for the produced particles. The rapidity dependence of the transverse momentum is also flat. We observe, that in the final state mesons cover a wider range in rapidity than quarks, which is due to the quark mean field.

More interesting than the $SU(2)$ case, which is presented here, is the extension to $SU(3)$. There it will be possible to verify the theoretical concepts for the production of strangelets or strangeness distillation. This will be the subject of an upcoming publication.

REFERENCES

- [1] *Proceedings of Quark Matter '96*, Eds. P. Braun–Munzinger, H. J. Specht, R. Stock and H. Stöcker, Nucl. Phys. A **610**, 1c (1997); *Proceedings of Quark Matter '97*, Nucl. Phys. A, in press.
- [2] J. D. Bjorken, Phys. Rev. D **27**, 140 (1983); J. Bolz, U. Ornik, M. Plümer, B. R. Schlei and R. M. Weiner, Phys. Rev. D **47**, 3860 (1993); D. H. Rischke and M. Gyulassy, Nucl. Phys. A **597**, 701 (1996).
- [3] Y. Nambu and G. Jona-Lasinio, Phys. Rev. **122**, 345 (1961); Y. Nambu and G. Jona-Lasinio, Phys. Rev. **124**, 246 (1961).
- [4] S. P. Klevansky, Rev. Mod. Phys. **64**, 649 (1992); T. Hatsuda and T. Kunihiro, Phys. Rep. **247**, 221 (1994).
- [5] W.-M. Zhang and L. Wilets, Phys. Rev. C **45**, 1900 (1992).
- [6] W. Florkowski, J. Hüfner, S. P. Klevansky and L. Neise, Ann. Phys. (NY) **245**, 445 (1995).
- [7] S. P. Klevansky, A. Ogura and J. Hüfner, Ann. Phys. (NY) **261**, 37 (1997).
- [8] P. Rehberg and J. Hüfner, Nucl. Phys. A **635**, 511 (1998).
- [9] P. Rehberg, Phys. Rev. C **57**, 3299 (1998).
- [10] A. Abada and J. Aichelin, Phys. Rev. Lett. **74**, 3130 (1995);
- [11] L. Bot and J. Aichelin, J. Phys. G **23**, 1947 (1997).
- [12] J. Gasser and H. Leutwyler, Ann. Phys. (NY) **158**, 142 (1984); J. F. Donoghue, E. Golowich and B. R. Holstein, *Dynamics of the Standard Model* (Cambridge University Press, 1992).
- [13] E. Laermann, Nucl. Phys. A **610**, 1c (1996); E. Laermann, Nucl. Phys. B (Proc. Suppl.) **60A**, 180 (1998).
- [14] J. Hüfner, S. P. Klevansky and P. Rehberg, Nucl. Phys. A **606**, 260 (1996).
- [15] J. Aichelin, Phys. Rep. **202**, 233 (1991).

- [16] See Ch. Hartnack, R.K. Puri, J. Aichelin, J. Konopka, S.A. Bass, H. Stöcker, W. Greiner, Euro. Phys. J. **1**, 151 (1998) and references cited therein.
- [17] E. Quack and S.P. Klevansky, Phys. Rev C **49**, 3283 (1994); J. Müller and S.P. Klevansky, Phys. Rev. C **50**, 410 (1994); V. Dmitrašinović, H.-J. Schulze, R. Tegen and R.H. Lemmer, Ann. Phys. (NY) **238**, 332 (1995).
- [18] P. Zhuang, J. Hüfner, S.P. Klevansky and L. Neise, Phys. Rev. D **51**, 3728 (1995); P. Rehberg, S.P. Klevansky and J. Hüfner, Nucl. Phys. A **608**, 356 (1996).
- [19] J. Hüfner, S.P. Klevansky, E. Quack and P. Zhuang, Phys. Lett. B **337**, 30 (1994).
- [20] P. Rehberg, S.P. Klevansky and J. Hüfner, Phys. Rev. C **53**, 410 (1996).

TABLES

r_0 (fm)	N_q	N_u	$N_{\bar{u}}$	N_d	$N_{\bar{d}}$	N_π	N_{π^0}	N_{π^+}	N_{π^-}
3	216	51.5	56.5	52	56	157	52.5	49.5	55
4	450	106.5	118.5	107.5	117.5	422	155	133	134
5	821	203.5	207	200	210.5	887.5	310	290.5	287
6	1283	320.5	321	319	322.5	1688.5	578	556	554.5
7	1931	480	485.5	482.5	483	2883.5	989	946	948.5

TABLE I. Multiplicity distribution in the final state as a function of the system size. The columns N_q and N_π give the sum over all quarks and all pions, respectively.

σ_h/σ_h^0	n_q	n_π	$n_\pi/(n_q + n_\pi)$
1	874	1126	0.563
2	708	1292	0.646
5	538	1462	0.731
10	420	1580	0.790

TABLE II. Particle multiplicity and ratio of pions to all particles for several calculations with artificially increased hadronization cross sections.

FIGURES

FIG. 1. Feynman graph for the irreducible pseudoscalar polarization. Solid lines denote constituent quarks.

FIG. 2. Mass spectrum of the $SU(2)$ NJL model in thermal equilibrium as a function of temperature. Solid line: quark mass times two, dashed line: pion mass, dot-dashed line: sigma mass.

FIG. 3. Feynman graphs for the process $qq \rightarrow qq$. Single lines denote quarks, double lines mesons. The graphs for the process $q\bar{q} \rightarrow q\bar{q}$ are obtained from these by a rotation around 90 degrees.

FIG. 4. Feynman graphs for the process $qq \rightarrow \pi\pi$. Single lines denote quarks, double lines mesons.

FIG. 5. Feynman graphs for the process $\pi \rightarrow q\bar{q}$. Single lines denote quarks, double lines mesons.

FIG. 6. Snapshot of the expansion of the fireball. Top: the system at $t = 0$, bottom: the same system at $t = 25 \text{ fm}/c$. Dark balls denote quarks, light balls denote pions.

FIG. 7. The constituent quark mass, averaged over all solid angles, as a function of r at different times.

FIG. 8. The effective temperature, averaged over all solid angles, as a function of r at different times.

FIG. 9. Mean radius of the fireball as a function of time for different expansion scenarios. Full line: full interaction, dashed line: Vlasov expansion, dotted line: free expansion.

FIG. 10. The particle density, averaged over all solid angles, as a function of r at different times. Solid lines: quarks, dashed lines: pions. Note the different scales on the vertical axes of the three rows.

FIG. 11. The particle multiplicity as a function of time. Solid line: quarks, dashed line: pions.

FIG. 12. Time dependence of the total number of collisions per time interval.

FIG. 13. Creation probability of pions as a function of the effective temperature. The Mott temperature is marked by the vertical line.

FIG. 14. Particle density summed over quarks and mesons along the coordinate axes. Upper panel: $t = 0$, lower panel: $t = 30 \text{ fm}/c$.

FIG. 15. Time dependence of the multiplicity for a system with cylindrically symmetric initial conditions. The solid line denotes quarks, the dashed line pions.

FIG. 16. Distribution of center points in rapidity for a system with cylindrically symmetric initial conditions. Upper panel: quark distribution in the initial state, lower panel: quark (+) and pion (\times) distribution in the final state. The lines are a guide to the eye only.

FIG. 17. Rapidity dependence of the mean transverse momentum for quarks in the initial state (+), quarks in the final state (\times) and pions in the final state (*).

FIG. 18. Energy density per particle for a fireball, in which a part of the quark momenta has been initialized according to a lower temperature. Solid line: ‘hot’ particles, dashed line: ‘cold’ particles. Please note the broken scale on the vertical axis.

$$-i\Pi_{PS}^R = \bullet \begin{array}{c} \xrightarrow{i\gamma^5\tau} \\ \xleftarrow{i\gamma^5\tau^\dagger} \end{array} \bullet$$

Figure 1

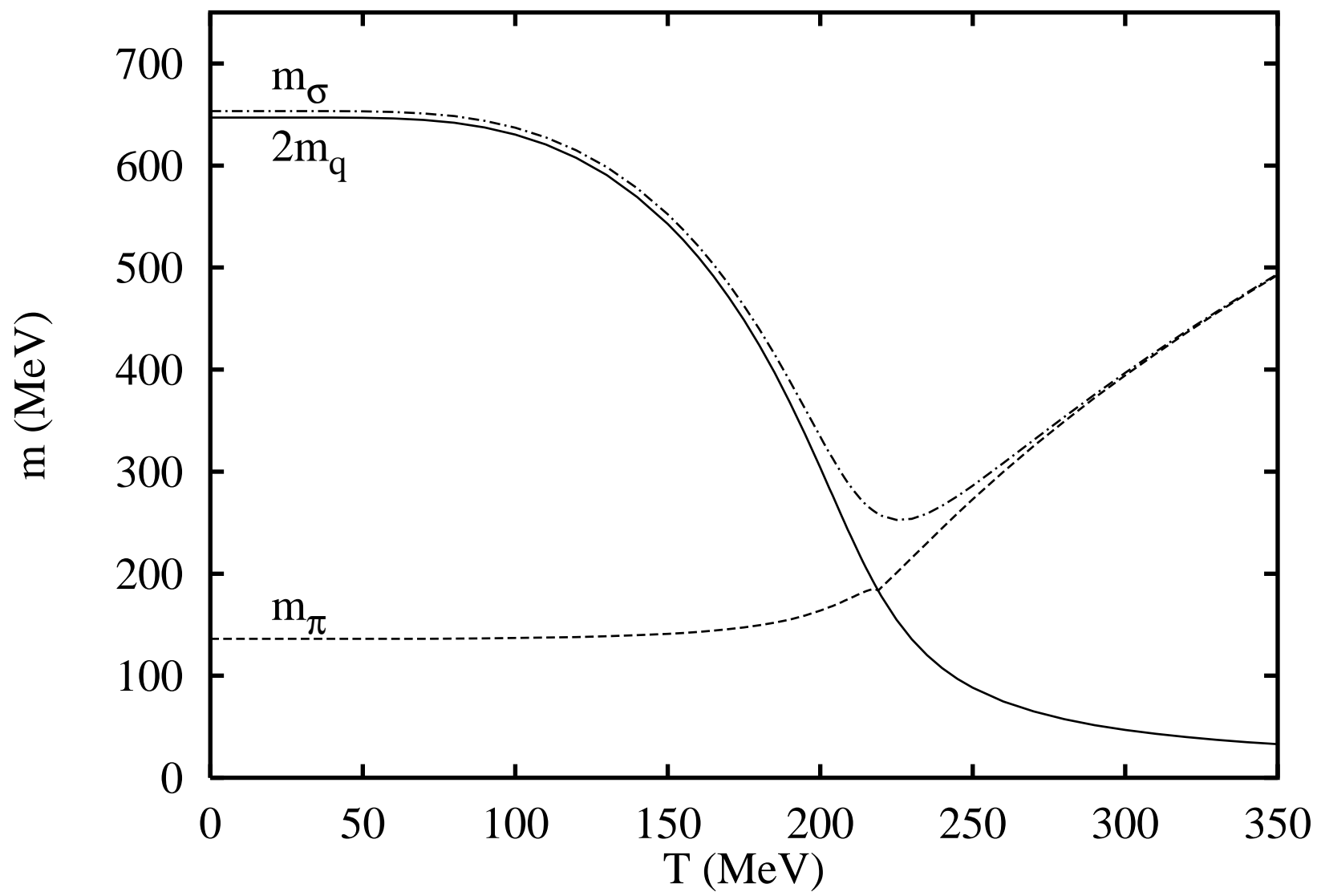


Figure 2

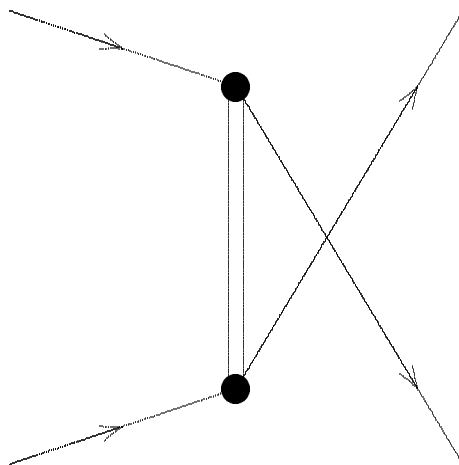
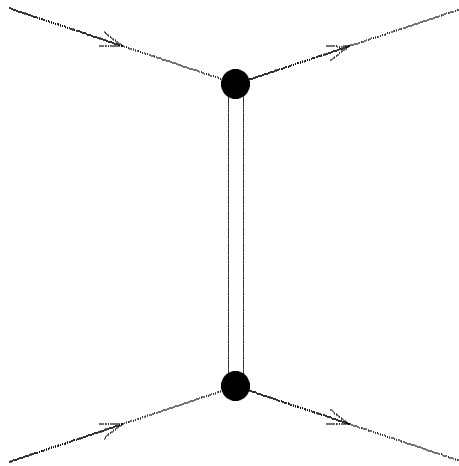


Figure 3

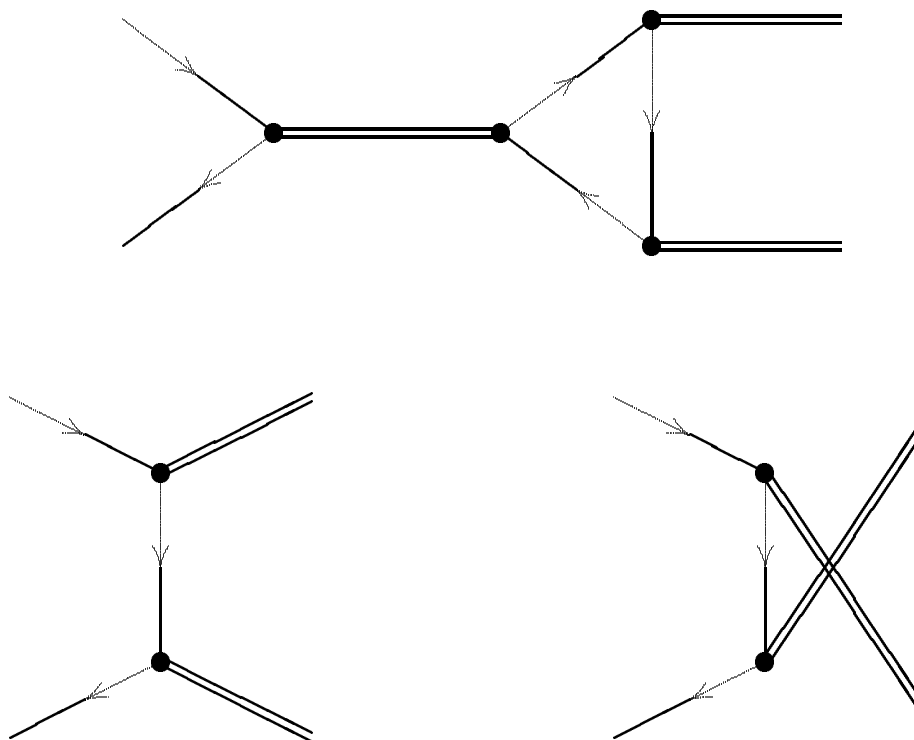


Figure 4

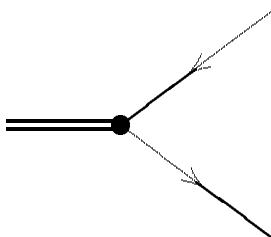


Figure 5

Figure 6

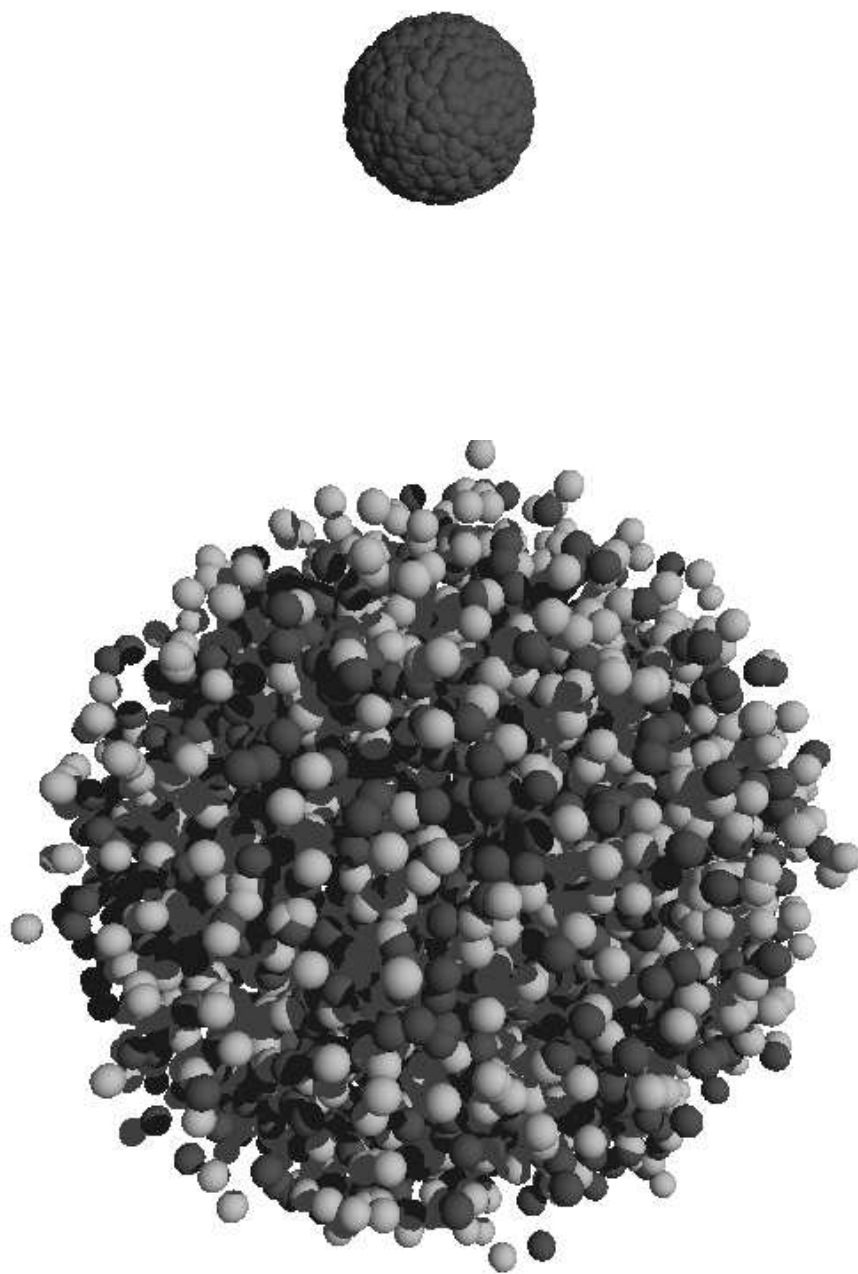


Figure 7

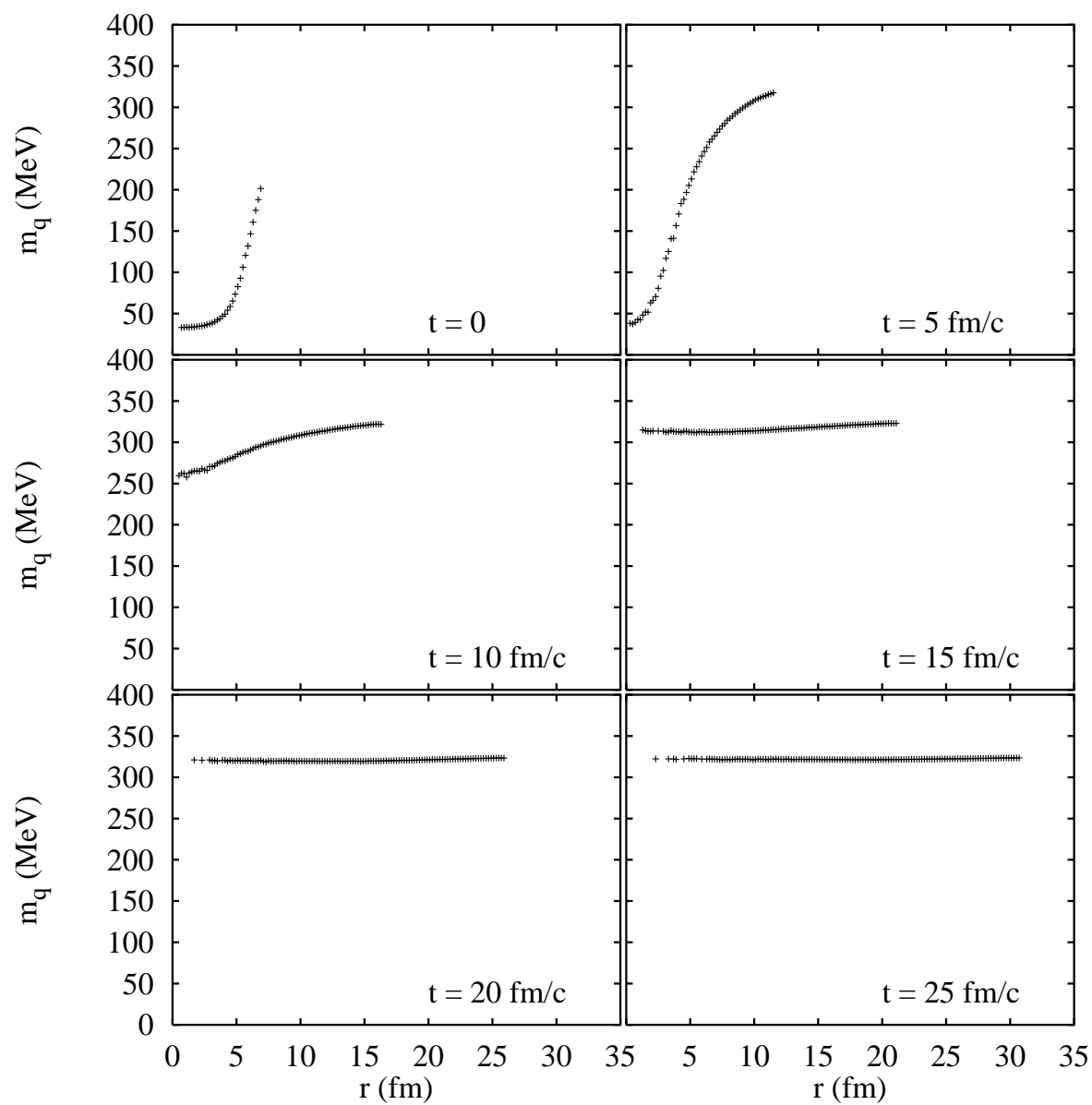
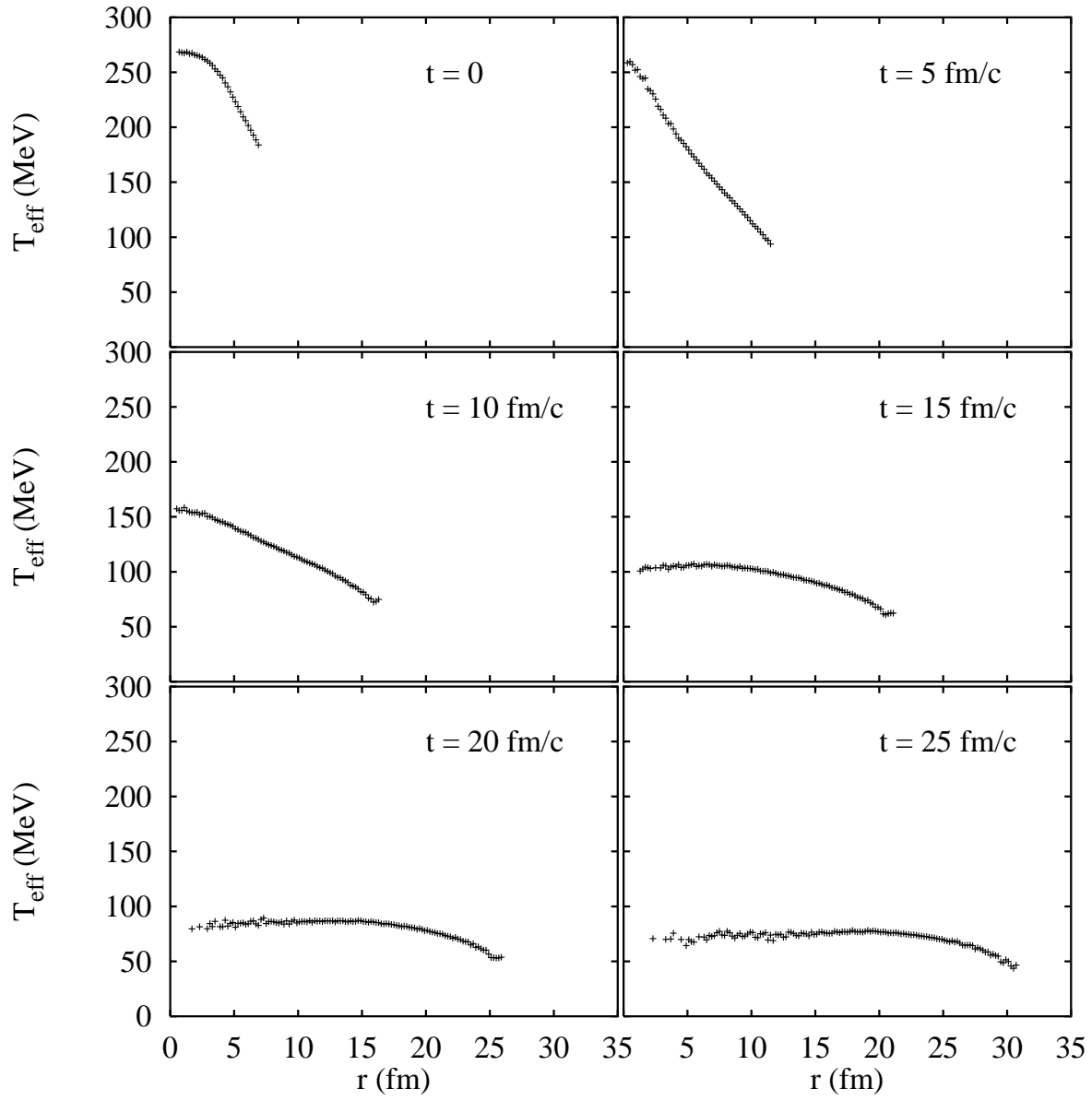


Figure 8



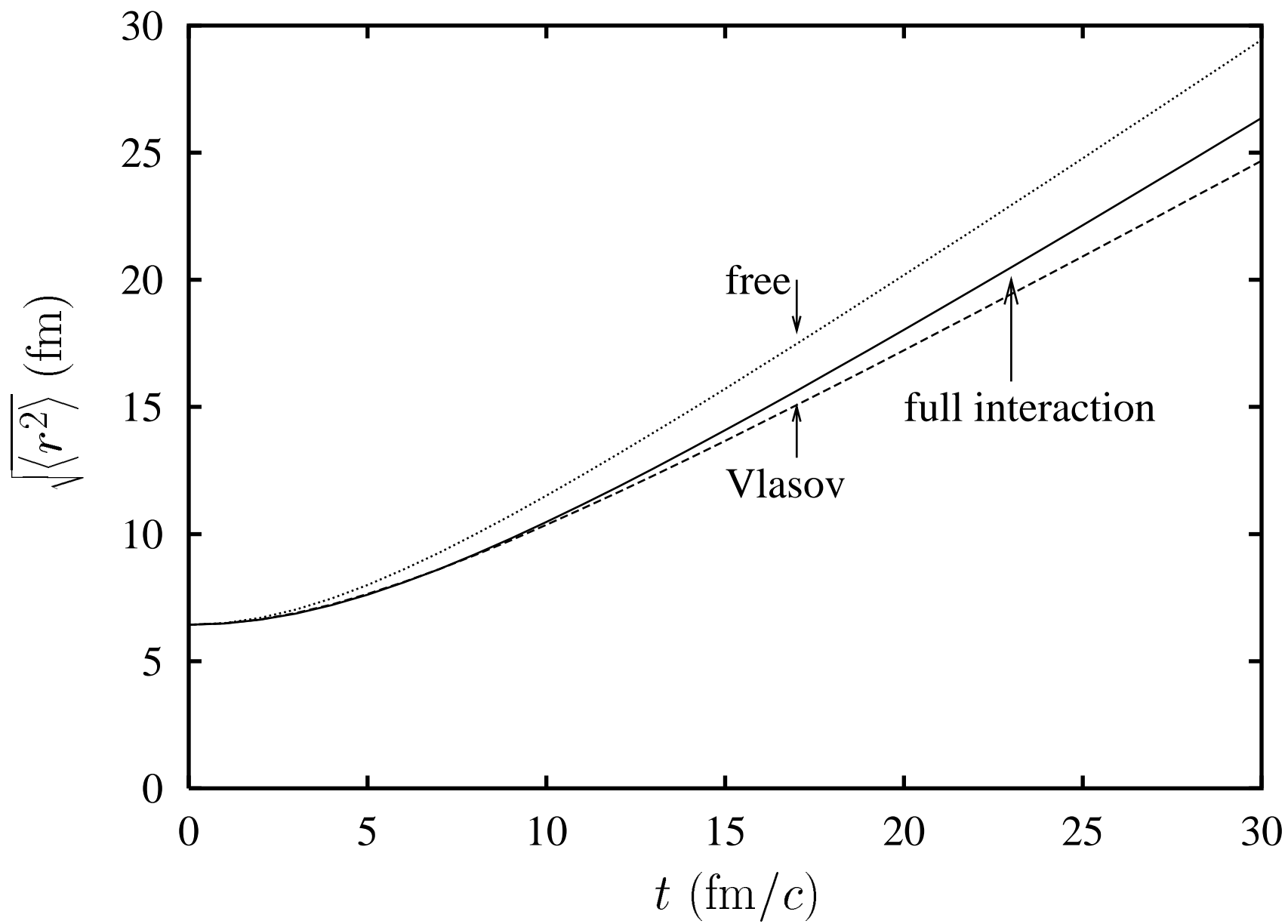
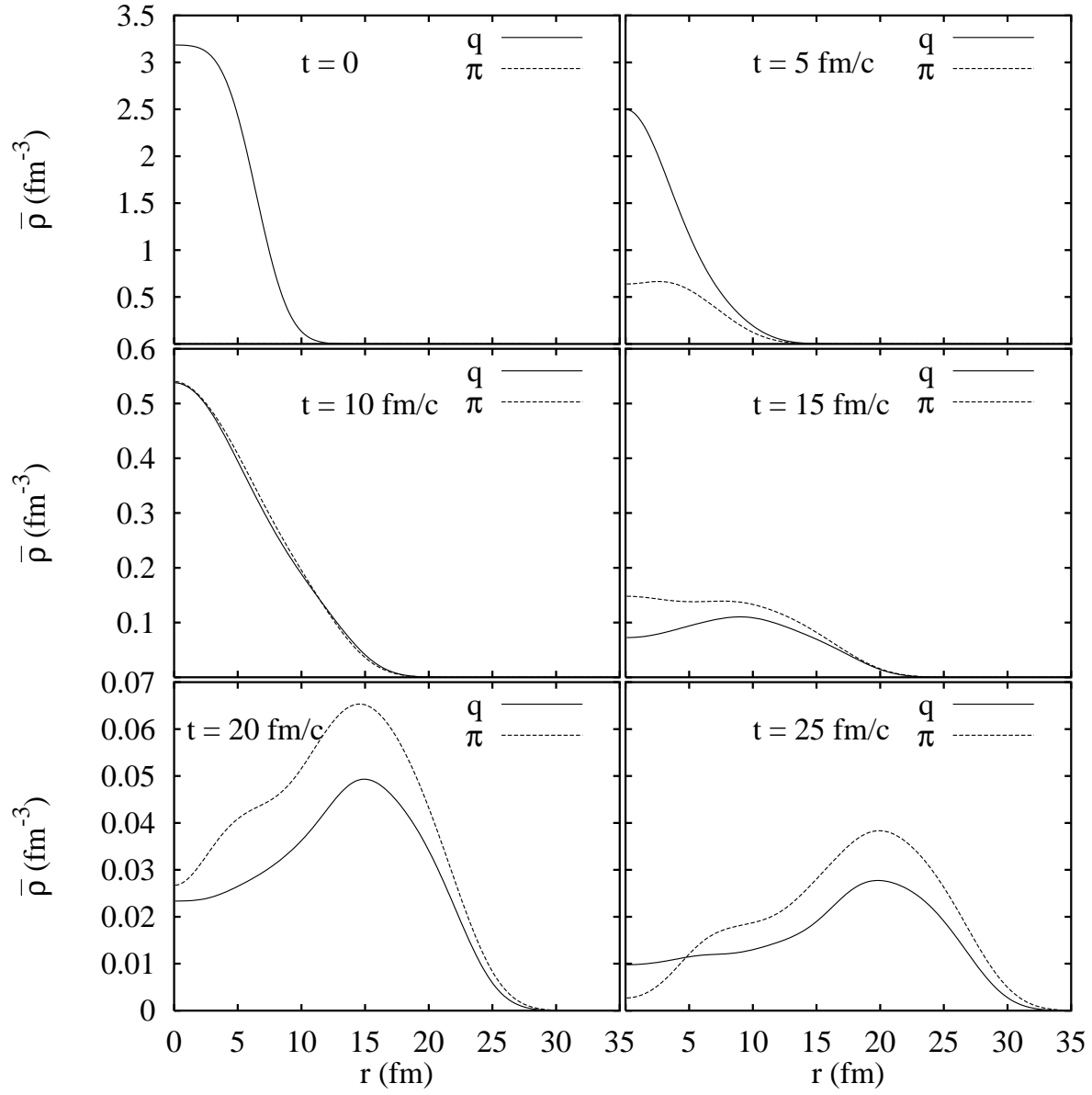


Figure 9

Figure 10



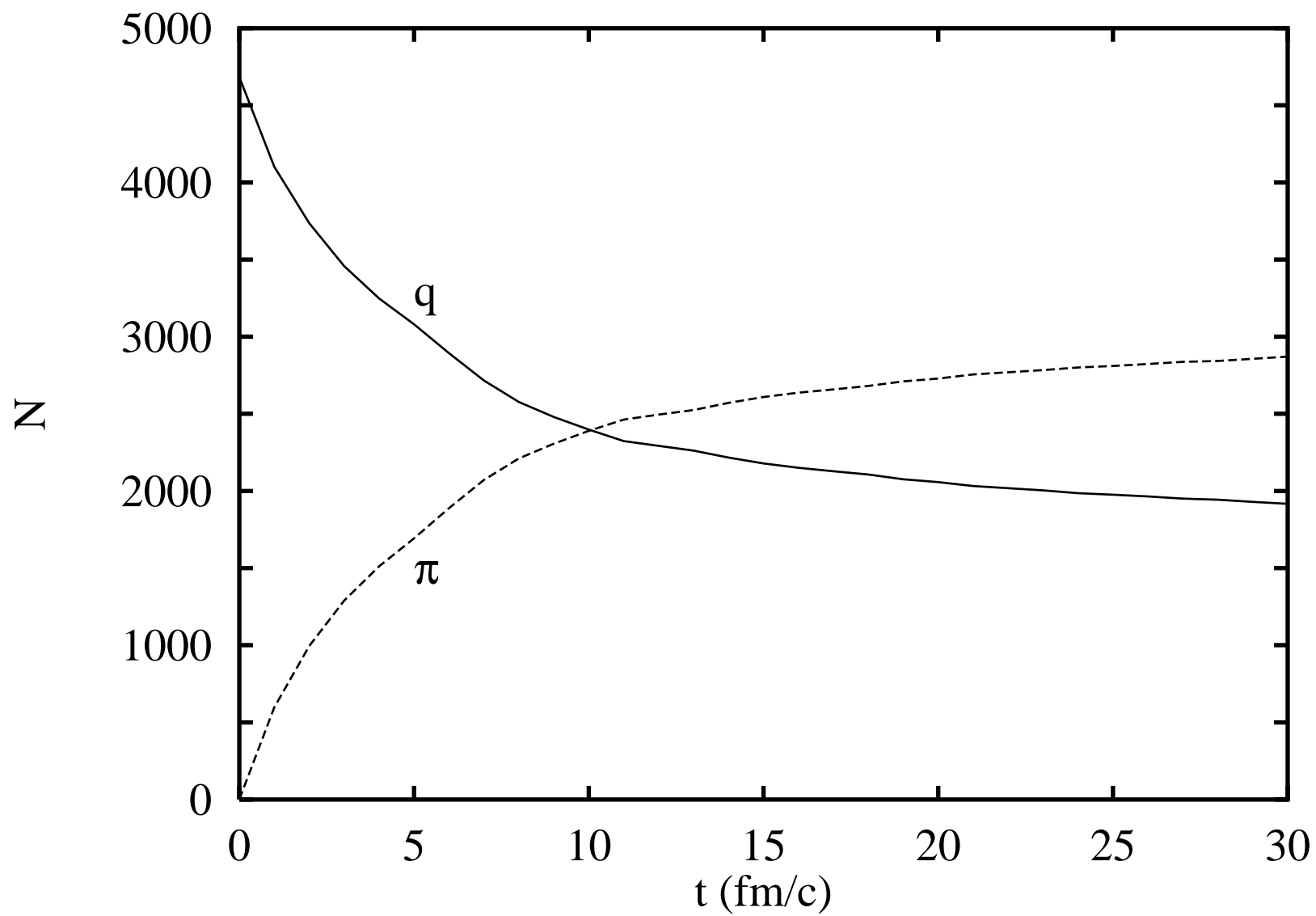


Figure 11

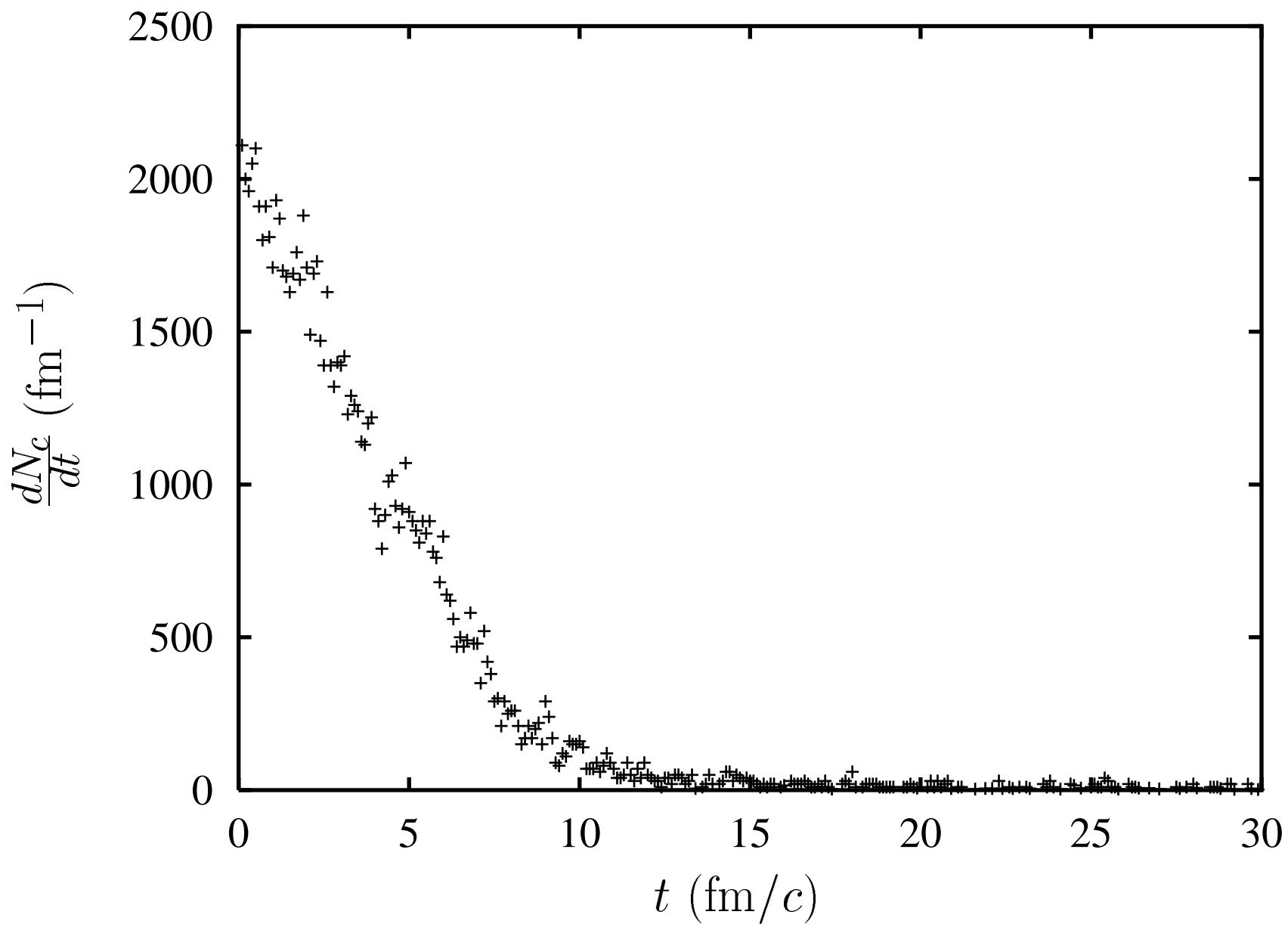


Figure 12

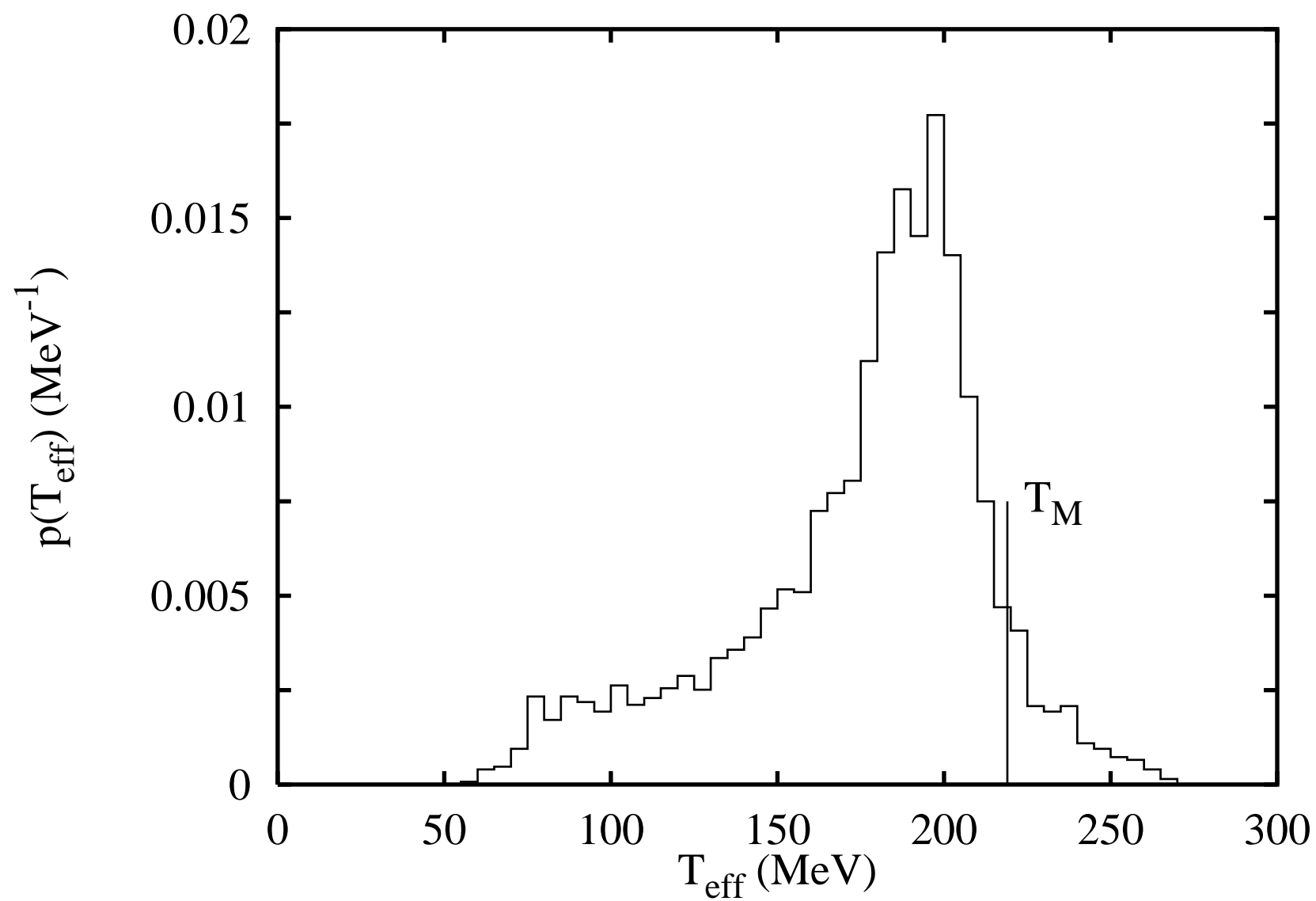
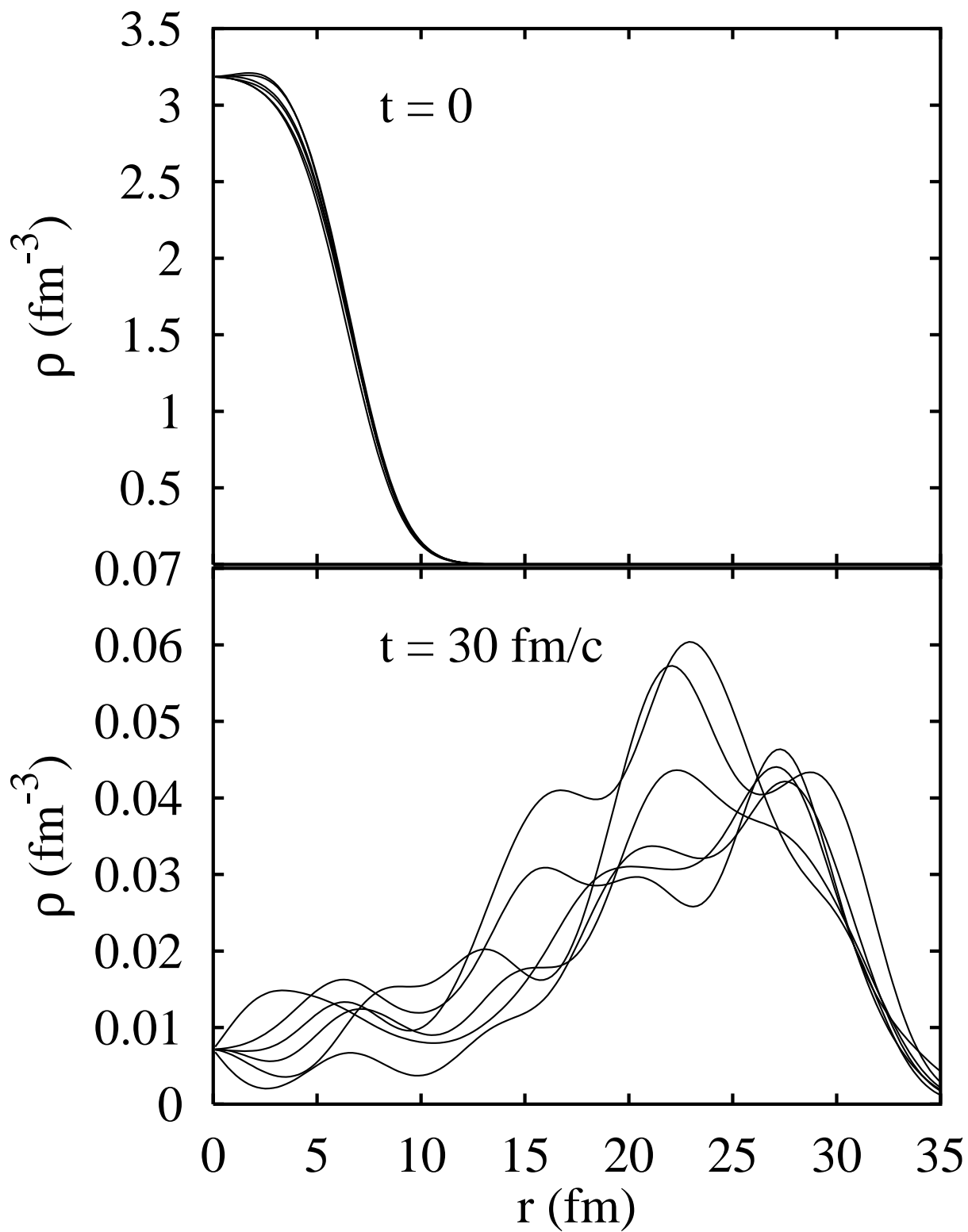


Figure 13

Figure 14



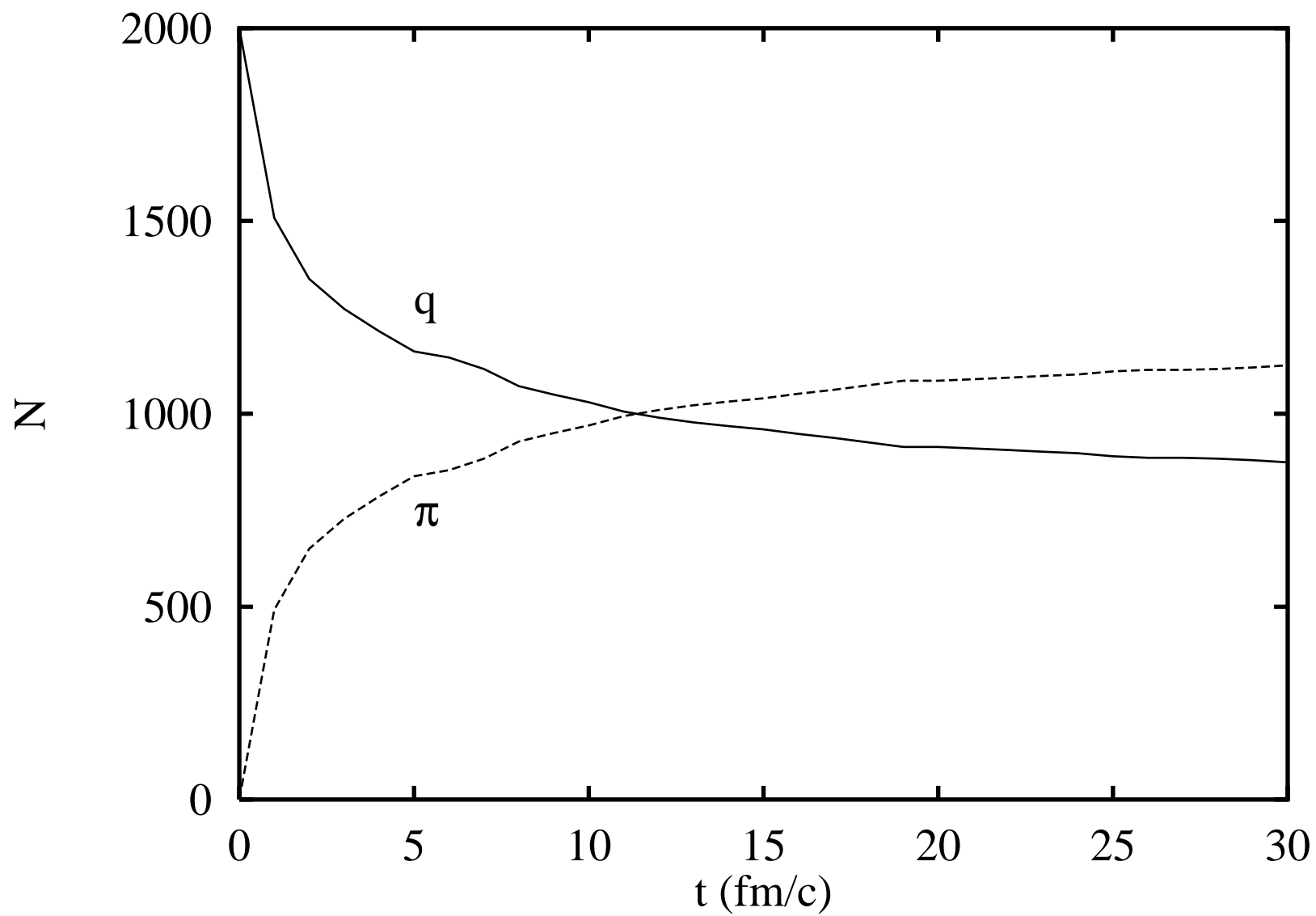
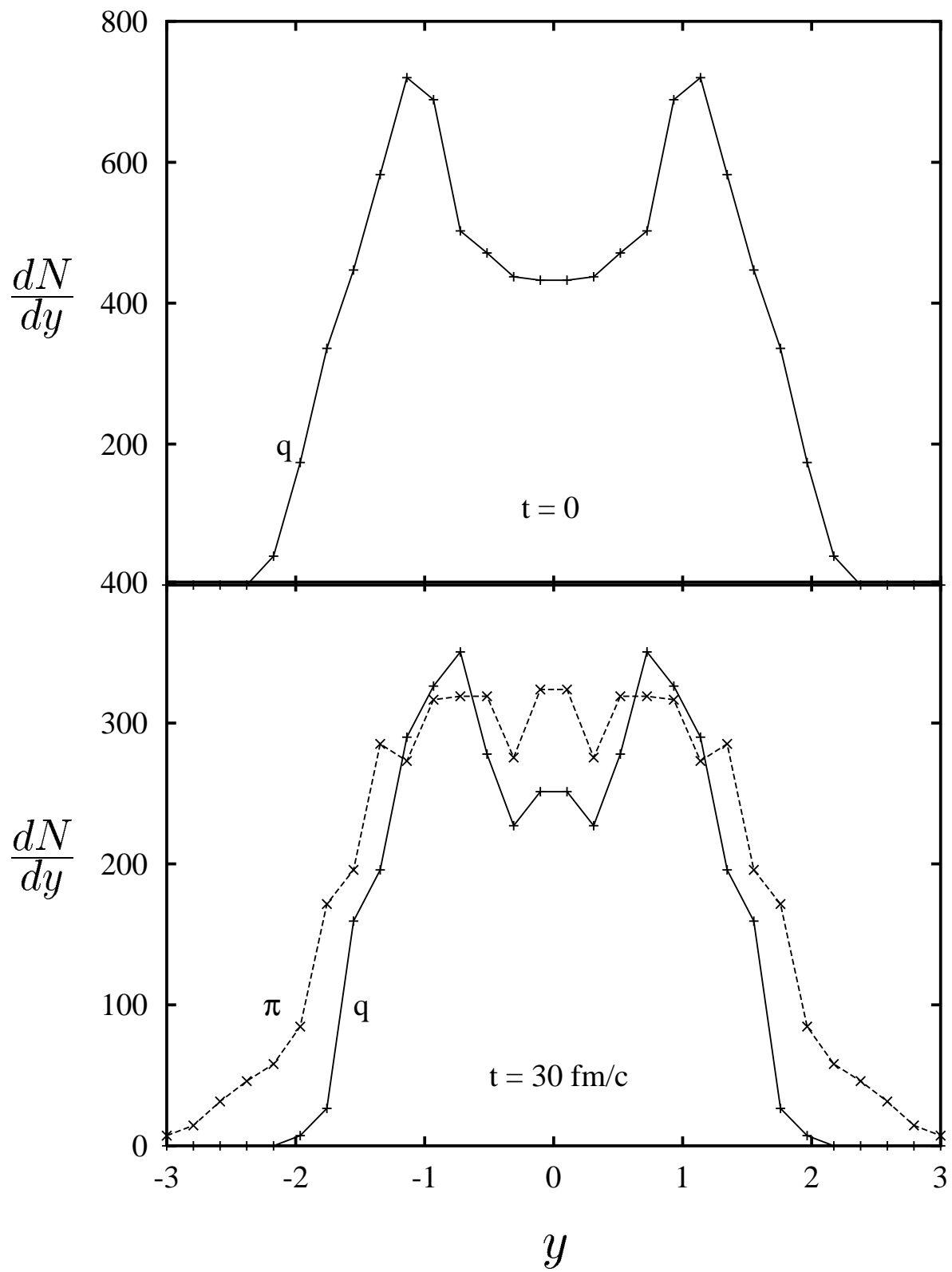


Figure 15

Figure 16



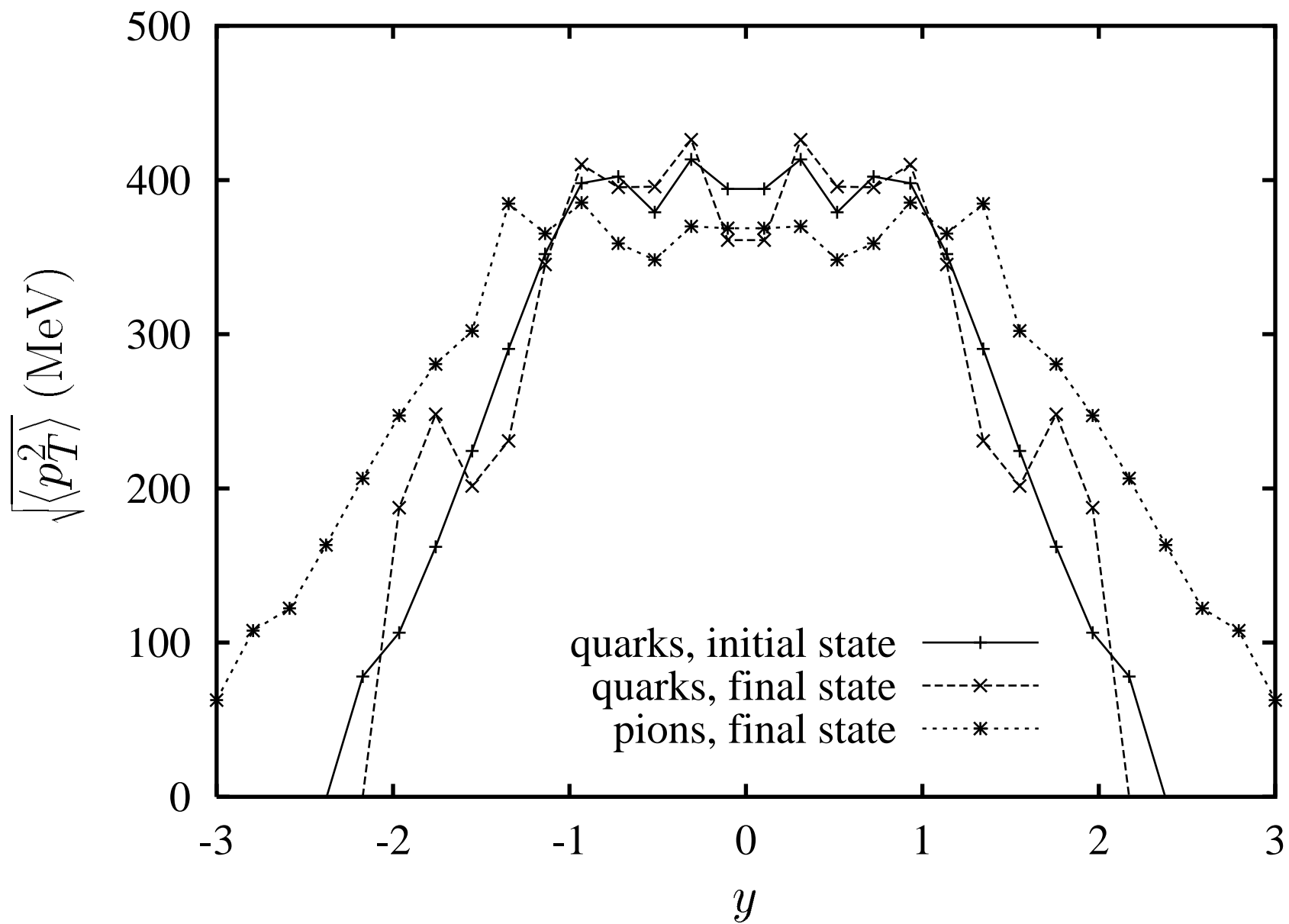


Figure 17

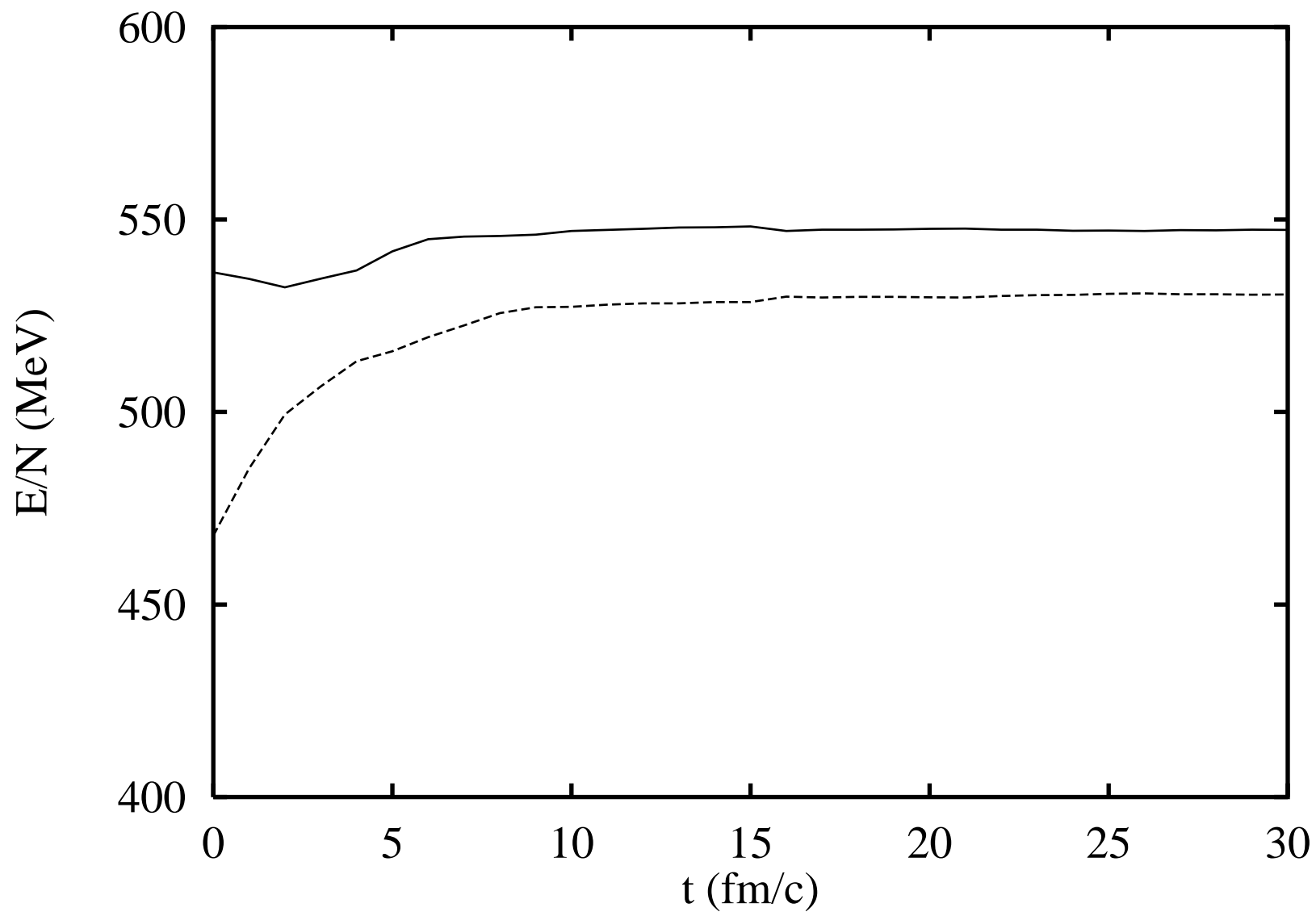


Figure 18